9

RESTRICTED

RM No. E7G11

CLASSIFICATION CHANGED TO

Authority Naca Form #36 Date

Dir., Aeron. Research
NACA

By D. Kay See Library

Westinghouse
J4C-2/2
pt. 1

NACA

JUL 31 1947

RESEARCH MEMORANDUM

for the

Bureau of Aeronautics, Navy Department

INVESTIGATION OF 10-STAGE AXIAL-FLOW X24C-2 COMPRESSOR. I - PERFORMANCE AT INLET PRESSURE OF 21 INCHES MERCURY ABSOLUTE AND INLET TEMPERATURE OF 538° R

By Harold J. Schum and Howard A. Buckner, Jr.

Flight Propulsion Research Laboratory
Cleveland, Ohio

CLASSIFIED DOCUMENT

This document contains classified information affecting the National Defense of the United States within the meaning of the Espionage Act, USC 50:31 and 32. Its transmission or the revelation of its contents in any manner to an unauthorized person is prohibited by law. Information so classified may be imparted only to persons in the military and naval Services of the United States, appropriate civilian officers and employees of the Federal Government who have a legitimate interest therein, and to United States citizens of known loyalty and discretion who of necessity must be informed thereof.

TECHNICAL EDITING WAIVED

UNCLASSIFIED

To W. Crowley per NACA Release form #2138

By authority of Exec. Dir. 10501 Date 12/14/53

Comk 1-11-54

CLASSIFICATION CHANGED

NATIONAL ADVISORY COMMITTEE FOR AERONAUTICS

WASHINGTON

JUL 15 1947

NACA LIBRARY
LANGLEY MEMORIAL AERONAUTICAL LABORATORY
Langley Field, Va.

RESTRICTED

RESTRICTED

 CONFIDENTIAL

NASA Technical Library
3 1176 01425 9619

NATIONAL ADVISORY COMMITTEE FOR AERONAUTICS

RESEARCH MEMORANDUM

for the

Bureau of Aeronautics, Navy Department

INVESTIGATION OF 10-STAGE AXIAL-FLOW X24C-2 COMPRESSOR

I - PERFORMANCE AT INLET PRESSURE OF 21 INCHES MERCURY ABSOLUTE AND INLET TEMPERATURE OF 538° R

By Harold J. Schum and Howard A. Buckner, Jr.

SUMMARY

An investigation is being conducted to determine the performance of the 10-stage axial-flow compressor from the X24C-2 turbojet engine. The performance of the compressor at an inlet pressure of 21 inches of mercury absolute and an inlet temperature of 538° R for percentages of equivalent design speed from 30 to 100 has been determined.

At the equivalent design speed of 12,000 rpm, the compressor produced a maximum pressure ratio of 3.44 at an equivalent weight flow of 54.0 pounds per second and an adiabatic temperature-rise efficiency of 0.803. This weight flow was within approximately 1 percent of the design value of 54.6 pounds per second but the pressure ratio was 14 percent lower than the design pressure ratio of 4. The peak adiabatic temperature-rise efficiency at equivalent design speed was 0.828 at a pressure ratio of 3.02 and an equivalent weight flow of 55.9 pounds per second. The compressor had a comparatively large surge-free operating range of weight flow for a given speed up to 89 percent of equivalent design speed. The peak adiabatic temperature-rise efficiency for a given speed generally occurred at values of pressure coefficient fairly close to 0.35. For this compressor, the efficiency data at the various speeds could be correlated on two converging curves by the use of a polytropic loss factor derived herein. The performance of the X24C-2 axial-flow compressor at the higher values of equivalent speed is summarized in the following table:

CONFIDENTIAL

RESTRICTED

Percentage equivalent design speed	Adiabatic temperature-rise efficiency	Pressure ratio	Mean pressure coefficient	Corrected air-weight flow (lb/sec)
At peak adiabatic temperature-rise efficiency				
100	0.828	3.02	0.338	55.9
89	0.846	2.60	0.360	48.4
80	0.827	2.19	0.354	41.1
72	0.812	1.91	0.356	33.7
At peak pressure ratio and peak pressure coefficient				
100	0.803	3.44	0.385	54.0
89	0.823	2.79	0.391	46.6
80	0.813	2.26	0.374	39.4
72	0.744	1.97	0.375	30.4

INTRODUCTION

At the request of the Bureau of Aeronautics, Navy Department, an investigation is being conducted at the NACA Cleveland laboratory to determine the performance characteristics of the 10-stage axial-flow compressor of the X24C-2 turbojet engine. This compressor was designed to handle 54.6 pounds of air per second at a pressure ratio of 4 with sea-level inlet conditions and a rotor speed of 12,000 rpm. The construction and setup of this investigation are similar to those of the 19B and 19XB compressors (references 1 and 2).

The performance of the compressor at the maximum constant inlet pressure obtainable with the laboratory exhaust facilities is presented herein. Subsequent reports of this investigation will present the separate effects of inlet pressure and inlet temperature on compressor performance, the result of surging studies, and material obtained from comprehensive interstage

measurements. For the phase of the investigation reported herein, runs with an inlet temperature of approximately 538° R were made at 30, 40, 47, 55, 65, 72, 80, and 89 percent of design speed at an inlet pressure of 21 inches of mercury absolute. At design speed, however, excess pressure drop through the compressor-inlet piping limited the inlet pressure to 19.5 inches of mercury absolute. At each speed runs were made over the entire range of surge-free air flows. Compressor pressure ratio, weight flow, adiabatic temperature-rise efficiency, pressure coefficient, and other performance characteristics as well as the results of interstage static-pressure measurements are presented.

COMPRESSOR

The X24C-2 compressor was designed for an air-weight flow of 54.6 pounds per second and a pressure ratio of 4 at 12,000 rpm with sea-level inlet conditions. The compressor consists of a row of inlet-guide vanes, 10 rows of rotor blades, nine rows of stator blades, and two rows of outlet-guide vanes. The pertinent blade data are given in table I. The compressor has a maximum over-all diameter of $23\frac{5}{8}$ inches at the outlet and is $44\frac{1}{8}$ inches in length from the inlet section to the outlet section. It is composed of three component parts: the inlet section, the stator casing, and the rotor.

Inlet section. - The cast-aluminum inlet section (fig. 1) of the X24C-2 compressor has an annular air passage with an inner and outer diameter of $7\frac{5}{8}$ and 21 inches, respectively. The length of the inlet section, exclusive of the inlet-guide vanes, is $6\frac{7}{8}$ inches. Four airfoil-shaped struts support the front bearing housing. Passages within these struts provide for the front bearing lubrication and the accessory drive.

The inlet-guide vanes are fully shrouded and the inner shroud is securely bolted to the rear of the inlet section. The inner and outer shrouds are tapered to provide a converging air passage from the inlet to the outlet of the blades. The inner-shroud diameter of the inlet-guide vanes increases from $7\frac{5}{8}$ to $9\frac{1}{2}$ inches and the outer-shroud diameter decreases from 21 to 19 inches, the stator-casing inner diameter. The inlet-guide vanes turn the air in the direction of rotor rotation. The 34 aluminum blades have a uniform chord length from base to tip. A hemispherical hub is attached to the entrance of the inlet section to provide smooth air entry into the compressor proper.

Stator casing. - The stator casing (fig. 2) is split into equal parts both axially and circumferentially. The casing has an inside diameter of 19 inches and circumferential grooves to support the nine stator and the two outlet-guide-vane diaphragms. The casing has an over-all flange-to-flange length of $37\frac{1}{4}$ inches.

The stator blades are stainless steel and are welded to the stainless-steel inner and outer shrouds. These shrouds are semicircular so each half can be easily mounted in the compressor-casing grooves. Two retaining screws hold each half of the diaphragm in place. Sheet-metal strips are welded to the inner shroud of each stator row of blades (fig. 2(b)) both at the inlet and the outlet to minimize backflow and to form air seals with machined shoulders on the rotor. The two rows of outlet-guide vanes are aluminum alloy and are peened to the inner and outer shrouds. From the outlet-guide vanes to the collector, the air passage forms a diverging outlet area. In order to simplify the compressor-outlet instrumentation in this investigation, the divergent area was straightened by installing a machined insert as recommended in reference 3.

Rotor. - The X24C-2 compressor rotor (fig. 3) is composed of 10 rotor disks that are slotted for blade mounting. The first nine disks are integral and are machined from a solid aluminum-alloy forging; the tenth rotor disk, made of steel, is bolted to the preceding nine rows. Metal is removed between each disk to decrease weight and to permit the adaptation of the stator-blade inner shrouds and the metal seal strips. The rotor has a constant inner diameter of 9.500 inches for the first two stages, after which the diameter gradually increases through the succeeding stages to 14 inches at the tenth row. This rotor has a constant diameter at the blade tips of 18.910 inches. The hub-tip ratios at the first and the last stages are 0.50 and 0.74, respectively.

The rotor blades are steel and are attached to the rotor by a bulb-type base in the same manner as the blades of the 19B and 19XB compressors (references 1 and 2). The blades decrease in height progressively from the inlet to the outlet of the compressor. A 0.045-inch clearance was maintained between the rotor-blade tips and the compressor casing. All rotor-blade tips are grooved to a radial depth of 7/64 inch to minimize damage to the compressor in case the blade tips rubbed the casing. An axial clearance of approximately 0.125 inch between stator and rotor blades was maintained.

SETUP AND INSTRUMENTATION

The setup used for the investigation of the X24C-2 axial-flow compressor is shown in figure 4. The compressor was driven by a 9000-horsepower variable-frequency induction motor rated at 1793 rpm, through a gear box with a step-up ratio of 8.974:1. The compressor and the collector were mounted on a pedestal that supported the unit at the inlet and the outlet sections.

Air entered a measuring orifice and duct through a butterfly throttle valve, and continued into a depression tank 6 feet in diameter and approximately 10 feet in length. Three screens were fitted into the midsection of the tank to remove any foreign particles and to insure a smooth air-flow distribution. A wood bellmouth was fitted between the depression tank and the compressor-inlet section to insure smooth air entry into the compressor. The air leaving the compressor passed through the straight annular outlet passage into the collector. Two 20-inch radial outlet pipes located diametrically opposite removed the discharge air from the collector to a common 20-inch pipe line connected into the laboratory altitude-exhaust facilities. A screen was welded into the outlet passage preceding the collector to decrease the possible circumferential pressure variations. The compressor-outlet pressure was regulated by a butterfly throttle valve located in the outlet pipe. Inlet-air piping, depression tank, compressor, and part of the outlet piping were lagged to minimize heat transfer between the working fluid and the ambient air.

The compressor rotor and the drive-shaft assembly used in this investigation are shown in figure 5. A splined coupling connected the gear box to the compressor, which was bolted to the compressor rotor through a rigid coupling. The unit had a three-bearing suspension; the front bearing was a thrust ball bearing and the other two were roller bearings. The front bearing was designed for a maximum thrust of 1500 pounds; to prevent operation above this value, the bearing outer race was held in a thrust-measuring device comparable to a metal bellows and mounted in the compressor-inlet section. Twelve strain gages were mounted in series on the parts of the thrust-measuring device subjected to strain. By previous calibration the axial movement of the rotating assembly and the strain on the front bearing could be determined. The strain was determined by measuring the resistance in millivolts across the strain-gage bridge on a potentiometer. A steel balance piston (fig. 5) was bolted to the rear of the compressor drive shaft and the two faces of the piston were sealed from other parts of the setup. High-pressure air

was admitted to the forward side of the piston to counteract the thrust developed by the compressor and to reduce the axial loading of the front bearing.

The air-weight flow through the compressor was measured by a calibrated, submerged, adjustable orifice located in a straight section of the inlet piping. The pressure drop across the orifice was determined by a water manometer; the upstream pressure was measured by a mercury manometer. Two iron-constantan thermocouples and two total-pressure tubes immediately upstream of the orifice were used to determine the state of the air entering the orifice. The entire compressor air-flow passage was sealed and the air flow necessary for the air-borne oil-mist lubrication system was metered in order to eliminate the air-leakage difficulties reported in reference 2.

A total-pressure rake consisting of five total-pressure tubes was used in conjunction with four wall static-pressure taps in the common 20-inch outlet pipe to check the air-weight flow downstream of the compressor. The total-pressure tubes across the pipe were located at the area centers of equal annular areas. The velocity pressure of the air flow was measured with water manometers. The outlet weight flow was used solely as a check for the inlet weight flow determined by the submerged orifice. Both air-measuring devices were previously calibrated against a standard orifice tank and an orifice. Because the measurements at the two stations agreed to within experimental error, only a negligible amount of air leakage existed at the particular value of inlet pressure investigated.

Inlet measurements were taken in the depression tank ahead of the compressor-inlet section, as recommended in reference 3. Two thermocouple rakes were inserted in the tank 180° apart. Each rake consisted of three thermocouples located at the centers of equal annular areas. Because of the large cross-sectional area of the tank, the velocity of the air through the tank was negligible and two static-pressure taps could be used to measure total pressure at the compressor inlet.

Static pressures before and after the inlet-section struts and after the inlet-guide vanes were measured. In order to obtain the pressure gradient through the compressor, the static pressure between each row of blades was determined by pressure taps in the compressor casing before and after each row of stator blades. These interstage pressures were taken in approximately the same longitudinal plane, each tap being centrally located between two

stator blades. Eight outlet static-pressure tubes and six thermocouples were located in the compressor-outlet section, as recommended in reference 3, to determine the compressor-outlet conditions.

Pressures were measured with water and with mercury manometers. All temperatures were taken with calibrated iron-constantan thermocouples. The difference in potential between the hot junction and the ice bath was measured with a sensitive calibrated potentiometer in conjunction with a spotlight galvanometer. The speed of the rotor was measured with an electric chronometric tachometer.

The precision of the measured and of the calculated quantities is estimated to be within the following limits:

Temperature, $^{\circ}$R	±0.5
Pressure, in. Hg	±0.05
Weight flow, percent	±1.0
Compressor speed, percent	±0.5
Pressure ratio, percent	±0.3
Efficiency, percent	±0.5[a]

[a]Accuracy for peak efficiency at design speed. At lower speeds where the temperature rise through the compressor is lower, the percentage of accuracy slightly decreased.

METHODS

The investigation to determine the performance characteristics of the X24C-2 axial-flow compressor was made at ambient-air temperature and the highest constant inlet-air pressure available. The inlet temperature varied from 528° to 543° R with an average value of 538° R. With an inlet-air pressure of 21 inches of mercury absolute, runs were made at 30, 40, 47, 55, 65, 72, 80, and 89 percent of design speed (12,000 rpm). Odd increments of speed were necessitated by the critical speeds encountered at 50, 60, and 90 percent of design speed. At design speed, excessive pressure drop in the inlet piping limited the maximum inlet pressure to 19.5 inches of mercury absolute. For each speed, the air-weight flow was varied from the maximum obtainable to the point just before incipient surging. Surge was detected audibly and by fluctuation in the manometers.

All data were corrected to NACA standard sea-level conditions (29.92 in. Hg and 518.4° R). The compressor-outlet total pressure

and all compressor-performance parameters were calculated in accordance with the recommendations of the NACA Subcommittee on Compressors (reference 3).

SYMBOLS

The following symbols are used in the calculations:

c_p	specific heat at constant pressure, (Btu/(lb)(°F))
c_v	specific heat at constant volume, (Btu/(lb)(°F))
D	inside diameter of compressor casing, (ft)
g	standard acceleration of gravity, 32.174 (ft/sec^2)
H	enthalpy corresponding to stagnation conditions, (Btu/lb)
J	mechanical equivalent of heat, 778.6 (ft-lb/(lb)(Btu))
M_2	outlet Mach number
m	polytropic exponent
n	number of stages
P_1	absolute inlet total pressure, (lb/sq ft)
P_2	absolute outlet total pressure, (lb/sq ft)
$(P_2/P_1)^{1/n}$	root-mean-pressure ratio per stage
p	absolute static pressure, (lb/sq ft)
p_x	absolute static pressure at various points along compressor casing, (lb/sq ft)
R	gas constant, 53.345 (ft-lb)/(lb)(°R) for dry air at 59° R
T_1	absolute inlet total temperature, (°R)
T_2	absolute outlet total temperature, (°R)

U	rotor speed at tip for first stage, (ft/sec)
$U_{i,1}$	rotor speed at hub for first stage, (ft/sec)
$U_{o,2}$	rotor speed at tip for last stage, (ft/sec)
$U_{i,2}$	rotor speed at hub for last stage, (ft/sec)
W	weight flow, (lb/sec)
$W\sqrt{\theta}/\delta$	weight flow corrected to NACA standard sea-level conditions, (lb/sec)
$W\sqrt{\theta}/\delta D^2$	specific equivalent flow rate corrected to NACA standard sea-level conditions, (lb/(sec)(sq ft))
γ	ratio of specific heats, c_p/c_v
$\triangle p$	increment of state function for polytropic process from inlet total pressure and temperature to outlet total pressure and temperature
δ	ratio of inlet-air total pressure to NACA standard sea-level pressure
η_p	polytropic efficiency, $\left(\frac{m}{m-1}\right)\Big/\left(\frac{\gamma}{\gamma-1}\right)$
$\triangle s$	increment of state function for isentropic process from inlet total pressure and temperature to outlet total pressure
η_T	adiabatic temperature-rise efficiency
θ	ratio of inlet-air total temperature to NACA standard sea-level temperature
λ_p	polytropic loss factor, $\frac{\Psi_m}{\eta_T}(1 - \eta_p)$
Ψ_m	mean pressure coefficient per stage
Ψ_m/η_T	work-input factor based on adiabatic temperature-rise efficiency
Ψ_p	polytropic pressure coefficient per stage

CALCULATIONS

The following equations were used to determine compressor parameters:

$$\Psi_m = \frac{J \Delta H}{\frac{n}{2}\left(\frac{U_{m,1}^2}{2g} + \frac{U_{m,2}^2}{2g}\right)}$$

where

$$U_{m,1} = \sqrt{\frac{1}{2}\left(U_{i,1}^2 + U^2\right)}$$

$$U_{m,2} = \sqrt{\frac{1}{2}\left(U_{i,2}^2 + U_{o,2}^2\right)}$$

The mean polytropic pressure coefficient per stage is computed in the same manner with the exception that the increment of state function for the polytropic process from inlet total pressure and temperature to outlet total pressure Δp is substituted for the corresponding value of the isentropic process Δs.

The polytropic exponent m was determined by substituting actual values of pressure and temperature in the equation

$$\left(\frac{T_2}{T_1}\right)^{\frac{m}{m-1}} = \left(\frac{P_2}{P_1}\right)$$

The polytropic energy addition to the gas is given by

$$\Delta p\, H = \frac{m}{m-1} R\, T_1 \left[\left(\frac{P_2}{P_1}\right)^{\frac{m-1}{m}} - 1\right] = \frac{m}{m-1} R(T_2 - T_1)$$

and the actual energy addition is given by

$$\Delta H = \frac{\gamma}{\gamma-1} R(T_2 - T_1)$$

The polytropic efficiency is then

$$\eta_p = \frac{\Delta p H}{\Delta H} = \left(\frac{m}{m-1}\right) \Big/ \left(\frac{\gamma}{\gamma-1}\right)$$

RESULTS AND DISCUSSION

General performance. - In the following discussion, all results are corrected to standard sea-level inlet conditions of pressure and temperature corresponding to 29.92 inches of mercury absolute and 518.4° R, respectively. The variation of over-all pressure ratio across the compressor P_2/P_1 and root-mean-pressure ratio per stage $(P_2/P_1)^{1/n}$ with weight flow $W\sqrt{\theta}/\delta$ and specific equivalent weight flow $W\sqrt{\theta}/\delta D^2$ is shown in figure 6 for several speeds. Figure 6(a) presents the compressor performance over the entire range of speeds investigated. Figures 6(b) and 6(c) show the low- and high-speed runs, respectively, on an enlarged scale in order that accurate values of mass flow and pressure ratio can be determined. Adiabatic temperature-rise efficiency contours and the surge line are also shown. Performance characteristics at peak pressure ratio, adiabatic efficiency, and pressure coefficient at the higher compressor speeds are given in the following table:

Percentage equivalent design speed	Adiabatic temperature-rise efficiency	Pressure ratio	Mean pressure coefficient	Corrected air-weight flow (lb/sec)
At peak adiabatic temperature-rise efficiency				
100	0.828	3.02	0.338	55.9
89	0.846	2.60	0.360	48.4
80	0.827	2.19	0.354	41.1
72	0.812	1.91	0.356	33.7
At peak pressure ratio and peak pressure coefficient				
100	0.803	3.44	0.385	54.0
89	0.823	2.79	0.391	46.6
80	0.813	2.26	0.374	39.4
72	0.744	1.97	0.375	30.4

The peak pressure ratio for a given compressor speed increased as the speed was increased. At the design speed, the maximum pressure ratio of 3.44 was obtained with an adiabatic temperature-rise efficiency of 0.803, an equivalent weight flow of 54.0 pounds per second, and a value of $W\sqrt{\theta}/\delta D^2$ of 21.5 pounds per second per square foot (figs. 6(c) and 7). The weight flow obtained was approximately 1 percent lower than the design weight flow of 54.6 pounds per second; this disagreement was within experimental error. The maximum pressure ratio obtained, however, was approximately 14 percent lower than the design pressure ratio of 4. The peak adiabatic temperature-rise efficiency at the design speed was 0.828 and was obtained at a pressure ratio of 3.02 and a corresponding flow of 55.9 pounds per second (figs. 7 and 8).

The theoretical maximum air flow calculated by assuming sonic velocity at the minimum area ahead of the first row of rotor blades is 62.8 pounds per second (fig. 6), which indicates that at the maximum flow of 56 pounds per second a choking condition at the inlet-guide vanes was being approached. The value of $W\sqrt{\theta}/\delta D^2$ of 21.6 at the maximum pressure ratio shows that this compressor has a very high flow capacity compared with other current compressors. The flow at maximum pressure ratio corresponds to about 56 percent of the value for sonic conditions ahead of the compressor where the full frontal area based on the rotor-tip diameter is used for the flow calculations.

The range of surge-free weight flow obtainable at a given speed increased with speed from 30 to 65 percent of design speed and decreased slightly with speed through 80 percent of design speed. The range at all these speeds was large, however, at a relatively constant pressure ratio. At 89 and 100 percent of the design speed, there was an abrupt decrease in the range of surge-free weight flow.

The pressure-ratio curves were limited at the lowest flow by surge for all speeds. The screen placed in the outlet of the compressor to insure uniform outlet conditions choked at slightly lower weight flows than did the compressor, thereby limiting the high-flow range of the pressure-ratio curves. The compressor was near a choking condition, however, because the curves were approaching a constant air-weight flow, particularly at the higher speeds. Consequently, the range of operation that is of interest was covered. The surge line is straight over the entire range of speeds investigated with the exception of the design speed, where the slope of the surge line increases. The straight part of the surge line passes through the point of zero mass flow and a pressure ratio of 1.0 and has a slope of approximately 0.039.

Adiabatic temperature-rise efficiency. - The variation of adiabatic temperature-rise efficiency with weight flow for all speeds investigated is shown in figure 7. The peak efficiency increased from 0.720 to 0.846 as the speed was increased from 30 to 89 percent of design speed; the peak efficiency at design speed dropped slightly to 0.828. The maximum adiabatic temperature-rise efficiency of 0.846 was obtained at a pressure ratio of 2.60 and a weight flow of 48.4 pounds per second. At a given speed, the efficiency increased to a peak value and then decreased as the weight flow was increased at speeds up to and including 80 percent of design speed. At 89 and 100 percent of design speed, the adiabatic temperature-rise efficiency was high and almost constant over the complete surge-free air-flow range, which shows that the compressor had not quite reached a choking condition. In general, the efficient surge-free operating range of the X24C-2 compressor for a given speed was comparatively large, especially at the lower speeds.

The variation of adiabatic temperature-rise efficiency with over-all pressure ratio for the speeds investigated is shown in figure 8. At each speed, the end of the curve with the higher pressure ratio is limited by surging. At 30 to 80 percent of design speed, the efficiency for a given speed increased with pressure ratio to the peak value and decreased as the equivalent weight flow was further decreased (fig. 6(a)). The efficiency continued to decrease with a further increase in pressure ratio until the peak pressure ratio was reached; at this point, both efficiency and pressure ratio decreased simultaneously. At 89 and 100 percent of design speed, an extremely large operating range of pressure ratio could be obtained with an almost constant high value of adiabatic temperature-rise efficiency.

Pressure coefficient. - The variation of the mean pressure coefficient per stage with equivalent weight flow for the compressor speeds investigated is shown in figure 9. Pressure coefficient is the ratio of the adiabatic energy addition to the gas to a constant times the square of the tangential velocity of some mean blade section in the compressor. It may be interpreted as a measure of the work done on the gas in an ideal process, brought to a nondimensional basis by dividing by the square of a mean tangential velocity. At speeds from 30 to 80 percent of design speed, the pressure coefficient for a given speed increased to a maximum and then decreased as the weight flow was increased. At 89 and 100 percent of design speed, however, the pressure coefficient continually decreased as the weight flow was increased. The lowest flow point of all the curves was limited by surge. The

peak pressure coefficient decreased from 0.43 to 0.37 in going from 30 to 80 percent of design speed; at 89 and 100 percent of design speed, the peak pressure coefficient increased to approximately 0.39 for both speeds. The gradual decrease followed by the sudden increase in the peak pressure coefficient with increasing speed is probably due to the differences in matching of the individual stages. The peak values of pressure coefficient for a given speed naturally occurred at the same values of weight flow as did the peak pressure ratio (fig. 6), because the two functions are directly related. The peak values of pressure ratio at each speed investigated occurred at values of pressure coefficient in the proximity of 0.40.

At each speed, the peak adiabatic temperature-rise efficiency occurred at values of the pressure coefficient fairly close to 0.35, as shown in figure 10, which is a cross plot of figures 7 and 9. The pressure coefficient also appears to govern the magnitude of the efficiency when the loading of the compressor blades is small; that is, in the high-flow regions at the low speeds (on the left side of figure), the data of figure 10 can be represented by a single curve. Apparently, the efficiency in the high-flow region for the low speeds is largely dependent on the ideal work done by the blades rather than the matching of the stages.

Work-input factor. - The variation of work-input factor based on adiabatic temperature-rise efficiency Ψ_m/η_T with equivalent weight flow for the various speeds is shown in figure 11. Work-input factor is the ratio of the actual energy addition to the gas to a constant times the square of the tangential velocity of some mean blade section in the compressor and may be regarded as a measure of the actual work done on the gas brought to a nondimensional basis by dividing by the square of a mean tangential velocity. At each speed, the work-input factor decreased as the weight flow was increased. The peak work-input factor for a given speed decreased from 1.50 to 0.48 in going from 30 to 100 percent of design speed. Inasmuch as the contours of adiabatic temperature-rise efficiency and pressure coefficient when plotted against weight flow are similar (figs. 7 and 9), the general slope of the work-input factor curves at various speeds indicates that the efficiency decreased more rapidly than pressure coefficient in the low-flow ranges of operation. The peak pressure ratio for a given speed, occurred at values of the work-input factor from approximately 0.65 to 0.48 in going from 30 to 100 percent of design speed (figs. 6 and 11).

In the case of work-input factor, much better correlation of the data for different speeds was obtained by the use of polytropic

efficiency rather than adiabatic efficiency (fig. 12). Polytropic efficiency may be considered an indication of mean stage efficiency.

The work-input factor determines the point at which the peak polytropic efficiency of this compressor occurs. As shown in figure 12, the peak polytropic efficiency for all speeds occurred at a work-input factor of approximately 0.45. When the compressor blades are lightly loaded (high flows and low speeds, shown on left side of figure), or when the blades approach stalling (low flows and low speeds, shown on right side of figure), a single curve may be used to represent the data. The actual work done on the gas by the compressor thus seems to be an important factor in determining the mean-stage efficiency.

Loss factor. - If the polytropic pressure coefficient is considered a measure of the useful work done on the gas during the compression process and the work-input factor is regarded as a measure of the actual work, then the losses would be given by

$$\lambda_p = \text{actual work} - \text{useful work}$$

$$= \frac{\Psi_p}{\eta_p} - \Psi_p = \frac{\Psi_p}{\eta_p}(1-\eta_p) = \frac{\Psi_m}{\eta_T}(1-\eta_p)$$

where

$$\Psi_p = \frac{J\Delta_p H}{\frac{n}{2}\left(\frac{U_{m,1}^2}{2g} + \frac{U_{m,2}^2}{2g}\right)}$$

The polytropic loss factor determines to a large extent the polytropic efficiency regardless of speed, as shown in figure 13. All the data correlate reasonably well on two curves that converge as the maximum efficiency is approached. For this compressor, the maximum efficiency occurs at the point of minimum losses. Also, at the point of maximum efficiency, the two converging curves appear to be tangent to a line passing through a polytropic efficiency of 1.00 when the polytropic loss factor is 0. The points for low flows at low speeds fall on the curve on the right side of the figure and those for high flows at low speeds fall on the curve on the left side of the figure. At the higher speeds (89 and 100 percent of design speed), the points actually occurred at very near the maximum efficiency, because

the compressor had an almost constant high efficiency over the complete range obtained at these speeds. Although the data correlated reasonably well on the two previously mentioned curves, the efficiencies at the lower speeds actually never reached the maximum value. Consequently, at the lower speeds the curves actually obtained in the region of high efficiency are similar to that shown for 30 percent of design speed.

Outlet Mach number. - The variation of outlet Mach number with weight flow for the speeds investigated is presented in figure 14. The outlet Mach number was computed by the method given in reference 3, which is based on the axial component of the outlet-air velocity. Because a machined insert was located in the diffuser passage to give a constant-area outlet section and the outlet guide vanes of the X24C-2 compressor were designed to remove all whirl velocity, the values given are representative of the Mach numbers immediately behind the last row of outlet guide vanes in the actual engine installation. The Mach number at the diffuser outlet in the actual engine would, of course, be much smaller because of the larger outlet area.

For a given speed, the outlet Mach number increased as the weight flow was increased. The Mach number is almost constant at 0.28, the highest flow points for speeds from 65 to 100 percent of design speed. The approach to vertical of the slopes of the curves at the high-flow ends is an indication that the compressor was very near a choking condition when the mass flow was limited by the screen in the outlet section, as previously mentioned. The outlet Mach number was 0.23 at the point of maximum pressure ratio (3.44) obtained at the design speed. (See figs. 6 and 14.)

Interstage static pressures. - The axial distribution of static pressure measured along the compressor casing is shown in figure 15 for peak efficiencies for the speeds investigated. The term p_x/P_1 represents the ratio of the static pressure at different points along the compressor casing to the inlet total pressure. In general, there was a uniform rise in static pressure from the first rotor through the rest of the compressor. From 30 to 65 percent of design speed, the tenth rotor row appears to be acting like a turbine; that is, an actual pressure drop existed across the tenth row of rotor blades at the compressor casing. At the higher speeds, however, this rotor had a normal rise in static pressure. The pressure drop across the inlet-guide vanes became quite high as the speed was increased; at design speed, the pressure ratio across the inlet-guide vanes was 0.59, which is near

the critical pressure ratio. This low pressure ratio supports the fact that the maximum weight flow theoretically possible to pass through the inlet-guide vanes is 62.8 pounds per second (fig. 6).

SUMMARY OF RESULTS

An investigation of the performance of the X24C-2 10-stage axial-flow compressor at an inlet pressure of 21 inches of mercury absolute and an inlet temperature of 538° R produced the following results:

1. The performance characteristics obtained at the higher values of equivalent speed were as follows:

Percentage equivalent design speed	Adiabatic temperature-rise efficiency	Pressure ratio	Mean pressure coefficient	Corrected air-weight flow (lb/sec)
At peak adiabatic temperature-rise efficiency				
100	0.828	3.02	0.338	55.9
89	0.846	2.60	0.360	48.4
80	0.827	2.19	0.354	41.1
72	0.812	1.91	0.356	33.7
At peak pressure ratio and peak pressure coefficient				
100	0.803	3.44	0.385	54.0
89	0.823	2.79	0.391	46.6
80	0.813	2.28	0.374	39.4
72	0.744	1.97	0.375	30.4

2. At equivalent design speed, the compressor had a maximum pressure ratio of 3.44 at an equivalent weight flow of 54.0 pounds per second and an adiabatic temperature-rise efficiency of 0.803.

This weight flow checked the design value, 54.6 pounds per second, within approximately 1 percent, but the pressure ratio obtained was 14 percent lower than the design pressure ratio of 4. The peak adiabatic temperature-rise efficiency at the design equivalent speed was 0.828 obtained at a pressure ratio of 3.02, and an equivalent weight flow of 55.9 pounds per second.

3. The compressor had a comparatively large surge-free operating range of weight flow for a given speed at speeds up to 89 percent of design speed; at 89 and 100 percent of design speed, this range decreased appreciably.

4. The peak adiabatic temperature-rise efficiency for a given speed generally occurred at values of the pressure coefficient fairly close to 0.35.

5. At peak adiabatic temperature-rise efficiency for a given speed, there was generally a uniform rise in static pressure along the compressor casing from the first rotor row through the rest of the compressor. The tenth rotor row, however, appeared to be acting as a turbine at some of the lower speeds.

6. For this compressor, the efficiency data at the various speeds could be correlated on two converging curves by the use of a polytropic loss factor derived herein.

Flight Propulsion Research Laboratory,
National Advisory Committee for Aeronautics,
Cleveland, Ohio.

Harold J. Schum,
Mechanical Engineer.

Howard A. Buckner, Jr.,
Mechanical Engineer.

Approved:

Oscar W. Schey,
Mechanical Engineer.

Robert O. Bullock,
Mechanical Engineer.

jgm

REFERENCES

1. Roepcke, Fay A., Burtt, Jack R., and Medeiros, Arthur A.: Performance of Westinghouse 19B Six-Stage Axial-Flow Compressor. NACA MR No. E5K07, Bur. Aero., 1945.

2. Downing, Richard M., and Finger, Harold B.: Performance of the 19XB 10-Stage Axial-Flow Compressor. NACA RM No. E6L04, Bur. Aero., 1946.

3. NACA Subcommittee on Compressors: Standard Procedures for Rating and Testing Multistage Axial-Flow Compressors. NACA TN No. 1138, Sept. 1946.

TABLE I - DESIGN DATA FOR X24C

Blade row	Blade length (in.)		Chord length (in.)		Blade thickness (percent chord)		Number of blades	Approximate stagger angles (deg)			
	Leading edge	Trailing edge	Casing A-A	Hub C-C	Casing A-A	Hub C-C		Hub	C-C	B-B	A-A
I.G.V.[a]	6.067	4.862	1.525	1.525	5.51	5.51	34	10	13	17	20
1R[b]	4.750	4.750	1.720	1.717	9.42	14.55	17	21	23	32	35
1S[c]	4.750	4.750	1.249	1.248	8.96	8.96	24	24	28	32	36
2R	4.750	4.750	1.720	1.717	9.42	14.55	20	25	27	36	39
2S	4.750	4.750	1.122	1.233	9.00	9.08	30	17	19	31	38
3R	4.705	4.635	1.388	1.639	9.58	11.47	25	23	27	34	38
3S	4.666	4.598	.995	1.228	8.84	9.04	36	23	25	33	37
4R	4.535	4.367	1.388	1.639	9.58	11.47	26	24	28	34	38
4S	4.385	4.214	.995	1.228	8.84	9.04	38	26	28	36	40
5R	4.125	3.883	1.388	1.639	9.58	11.47	28	27	32	38	42
5S	3.910	3.747	.971	1.214	9.16	9.06	40	29	32	38	42
6R	3.675	3.484	1.267	1.481	9.78	11.82	34	30	33	40	42
6S	3.513	3.374	.971	1.214	9.16	9.06	42	32	34	40	44
7R	3.305	3.152	1.267	1.481	9.78	11.82	36	33	35	42	44
7S	3.184	3.065	.971	1.214	9.16	9.06	44	34	38	44	48
8R	3.000	2.850	1.267	1.481	9.78	11.82	38	35	36	43	45
8S	2.883	2.782	.810	1.007	10.87	9.33	60	34	35	42	46
9R	2.717	2.586	.994	1.260	9.46	11.75	49	34	37	43	47
9S	2.619	2.520	.810	1.007	10.87	9.33	62	35	36	43	47
10R	2.455	2.455	.994	1.260	9.46	11.75	49	37	40	46	50
O.G.V.[d]	2.512	2.637	1.000	1.000	9.00	9.00	62	46	46	46	46
O.G.V.[e]	2.653	2.822	1.000	1.000	9.00	9.00	76	14	14	14	14

NATIONAL ADVISORY
COMMITTEE FOR AERONAUTICS

[a]Inlet-guide vanes.
[b]Rotor.
[c]Stator.
[d]First row of outlet-guide vanes.
[e]Second row of outlet-guide vanes.
[f]Distance to section from point of intersection of mean axial line and blade base.

AXIAL-FLOW COMPRESSOR BLADES

NATIONAL ADVISORY
COMMITTEE FOR AERONAUTICS

Location of stagger angles (in.)			Leading-edge radius (in.)		Trailing-edge radius (in.)		Maximum thickness (in.)	
F	G	H	Casing A-A	Hub C-C	Casing A-A	Hub C-C	Casing A-A	Hub C-C
1.016[f]	1.750	1.750	0.037	0.037	0.005	0.005	0.090	0.090
.375	2.000	2.000	.036	.055	.005	.005	.162	.250
.375	2.000	2.000	.025	.025	.005	.005	.112	.112
.375	2.000	2.000	.036	.055	.005	.005	.162	.250
.375	2.000	2.000	.023	.025	.005	.005	.101	.112
.875	1.500	1.500	.029	.041	.005	.005	.133	.188
.313	2.000	1.500	.019	.025	.005	.005	.088	.111
.875	1.500	1.500	.029	.041	.005	.005	.133	.188
.313	2.000	1.500	.019	.025	.005	.005	.088	.111
.875	1.500	1.500	.029	.041	.005	.005	.133	.188
.418	1.500	1.500	.020	.025	.005	.005	.089	.110
.359	1.500	1.000	.028	.038	.005	.005	.124	.175
.418	1.500	1.500	.020	.025	.005	.005	.089	.110
.359	1.500	1.000	.028	.038	.005	.005	.124	.175
.418	1.500	1.500	.020	.025	.005	.005	.089	.110
.359	1.500	1.000	.028	.038	.005	.005	.124	.175
.410	1.000	1.000	.019	.021	.005	.005	.088	.094
.375	1.000	1.000	.021	.033	.005	.005	.094	.148
.410	1.000	1.000	.019	.021	.005	.005	.088	.094
.375	1.000	1.000	.021	.033	.005	.005	.094	.148
----	-----	-----	.020	.020	.005	.005	.090	.090
----	-----	-----	.020	.020	.005	.005	.090	.090

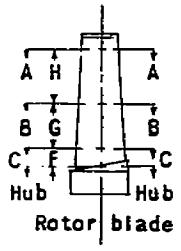

Rotor blade

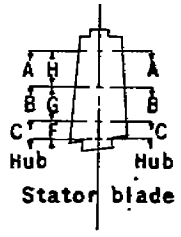

Stator blade

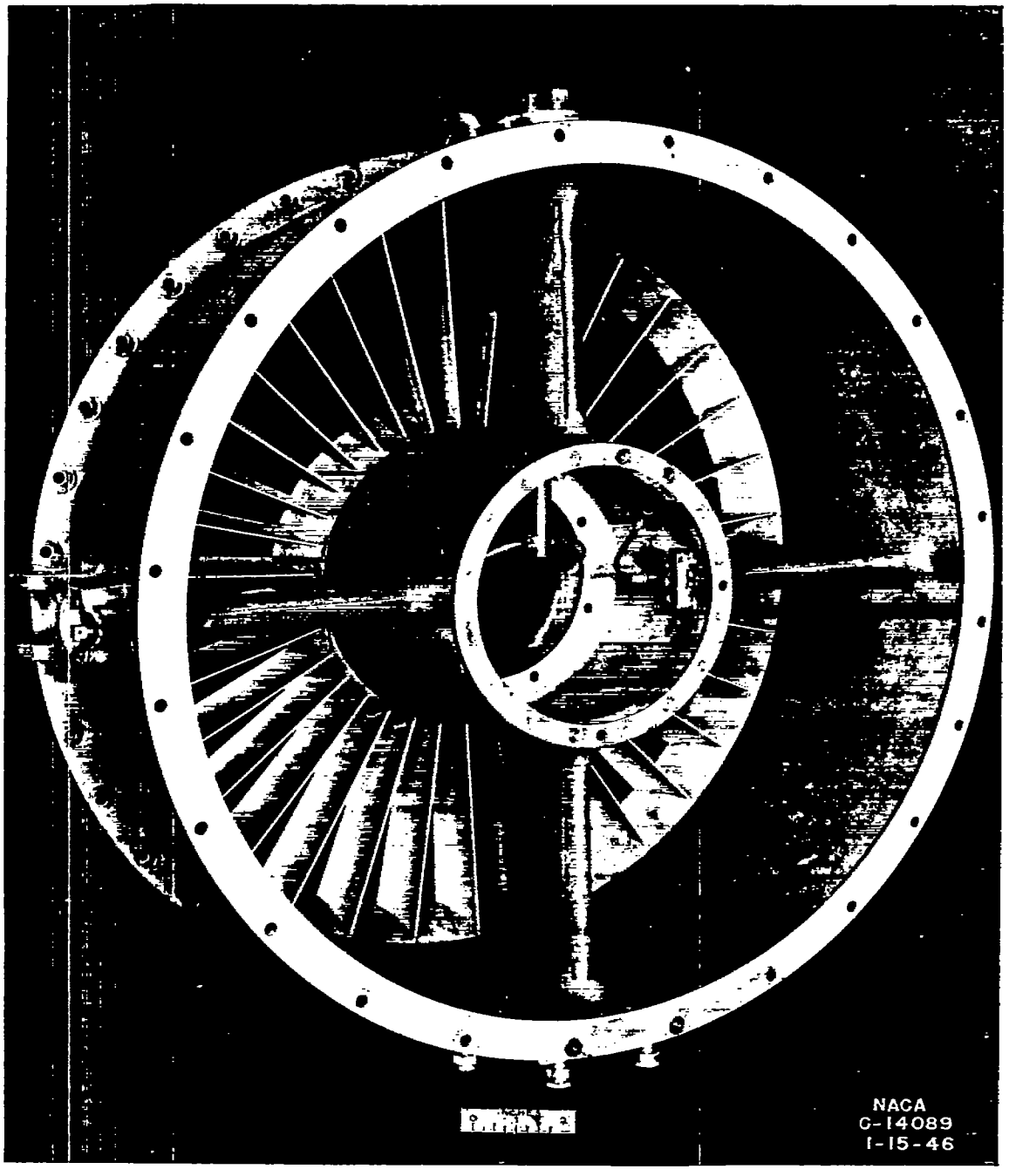

Figure 1. - Front view of inlet section of X24C-2 axial-flow compressor.

[redacted]

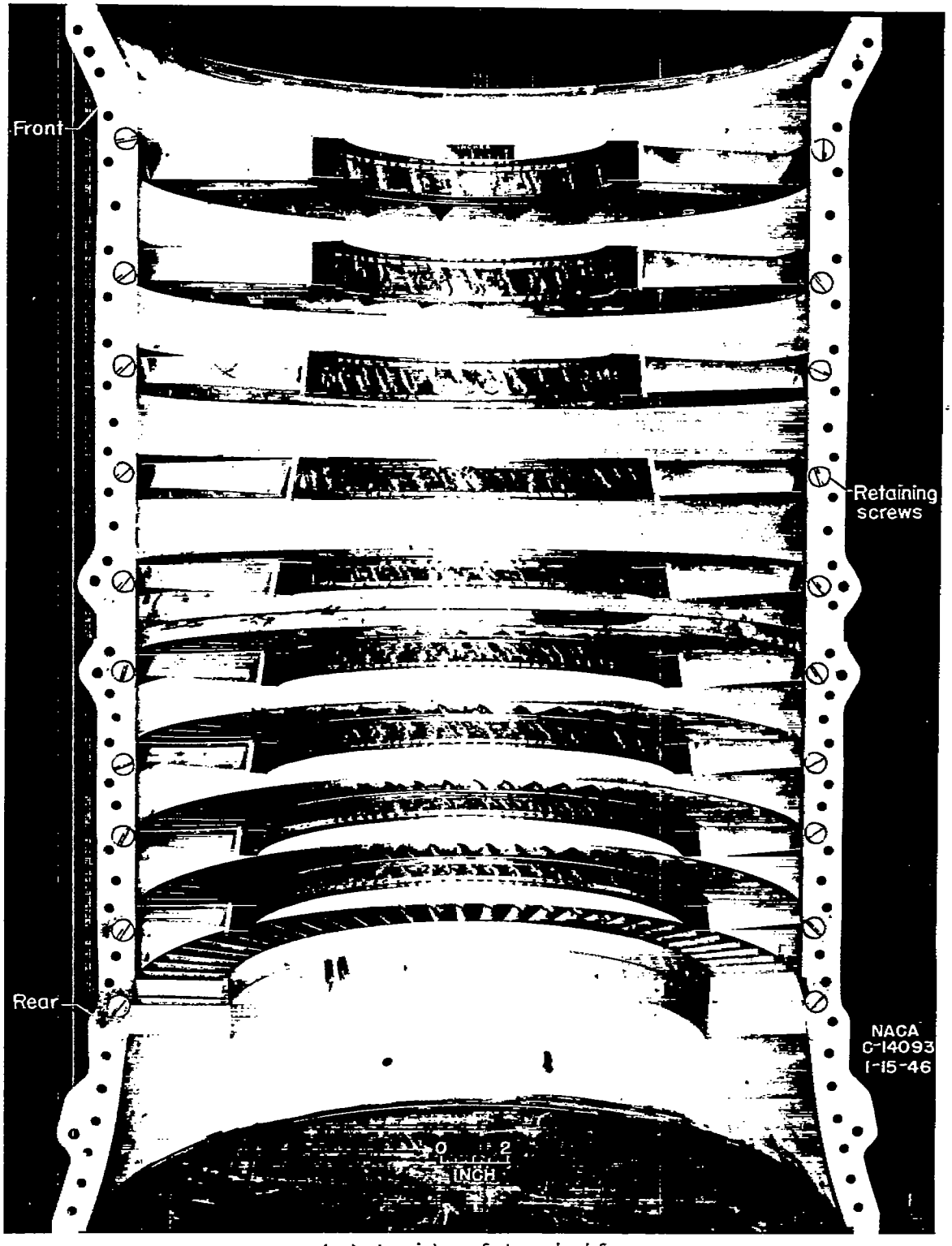

(a) Inside of top half.

Figure 2. - Stator casing for X24C-2 axial-flow compressor.

[redacted]

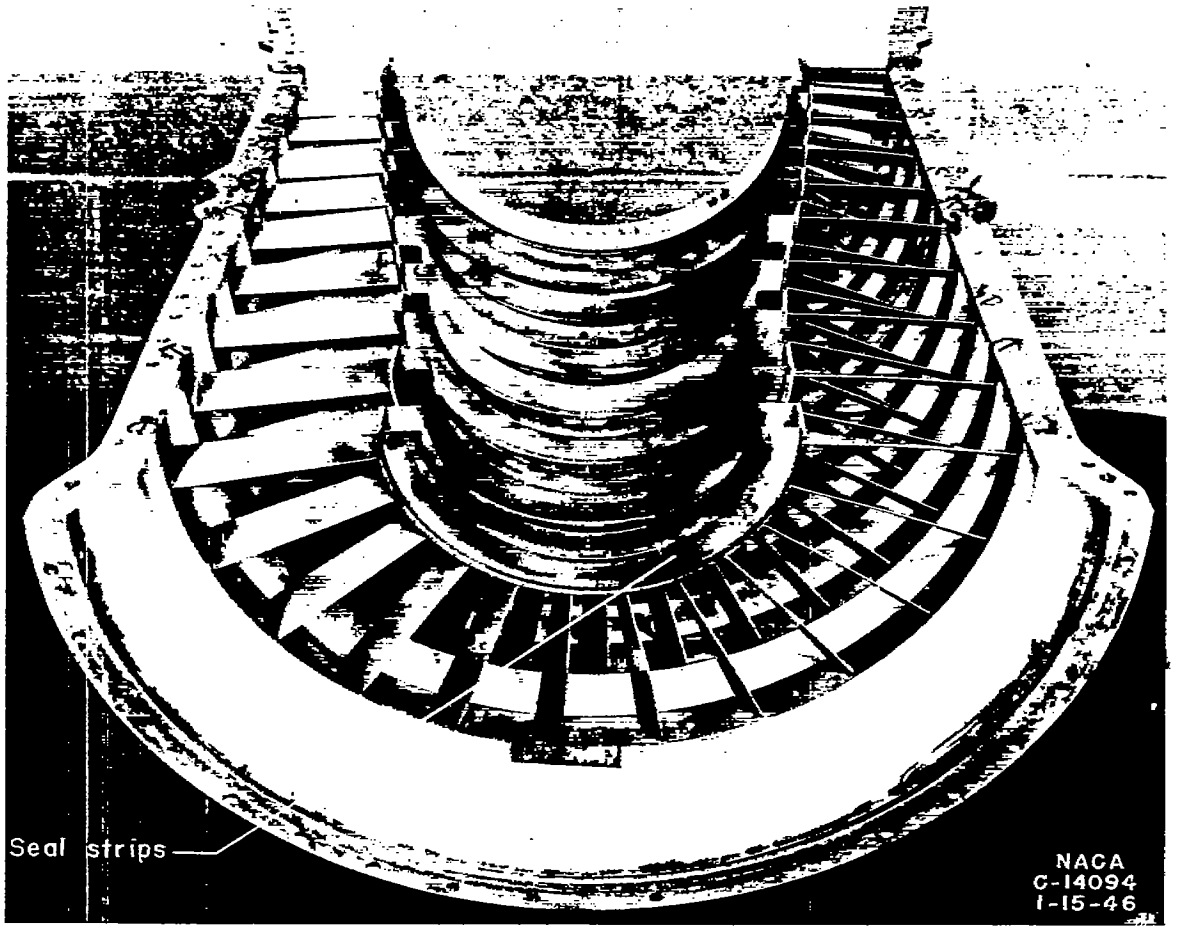

(b) Front of top half.

Figure 2. - Concluded. Stator casing for X24C-2 axial-flow compressor.

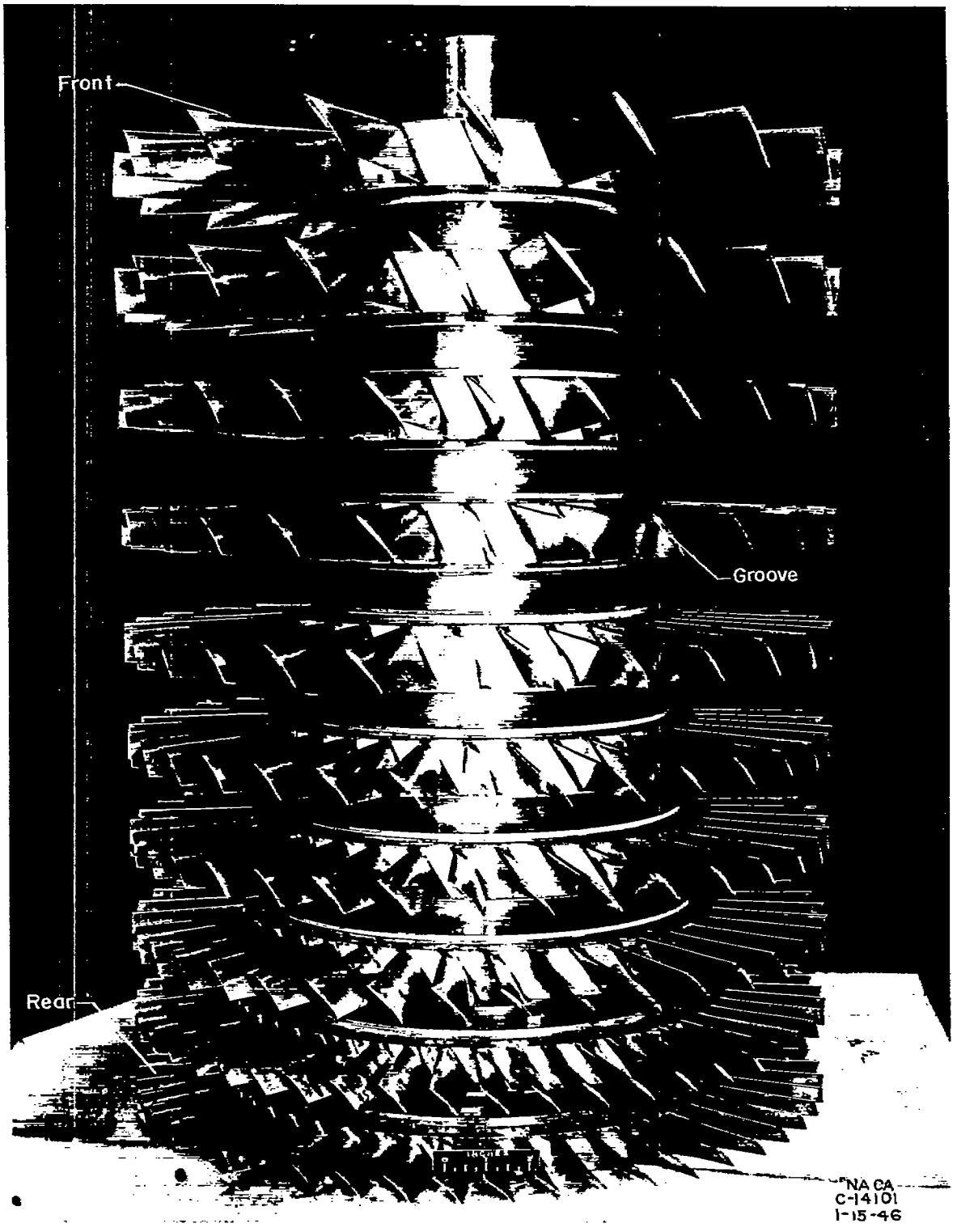

Figure 3. - Rotor for X24C-2 axial-flow compressor.

[redacted]

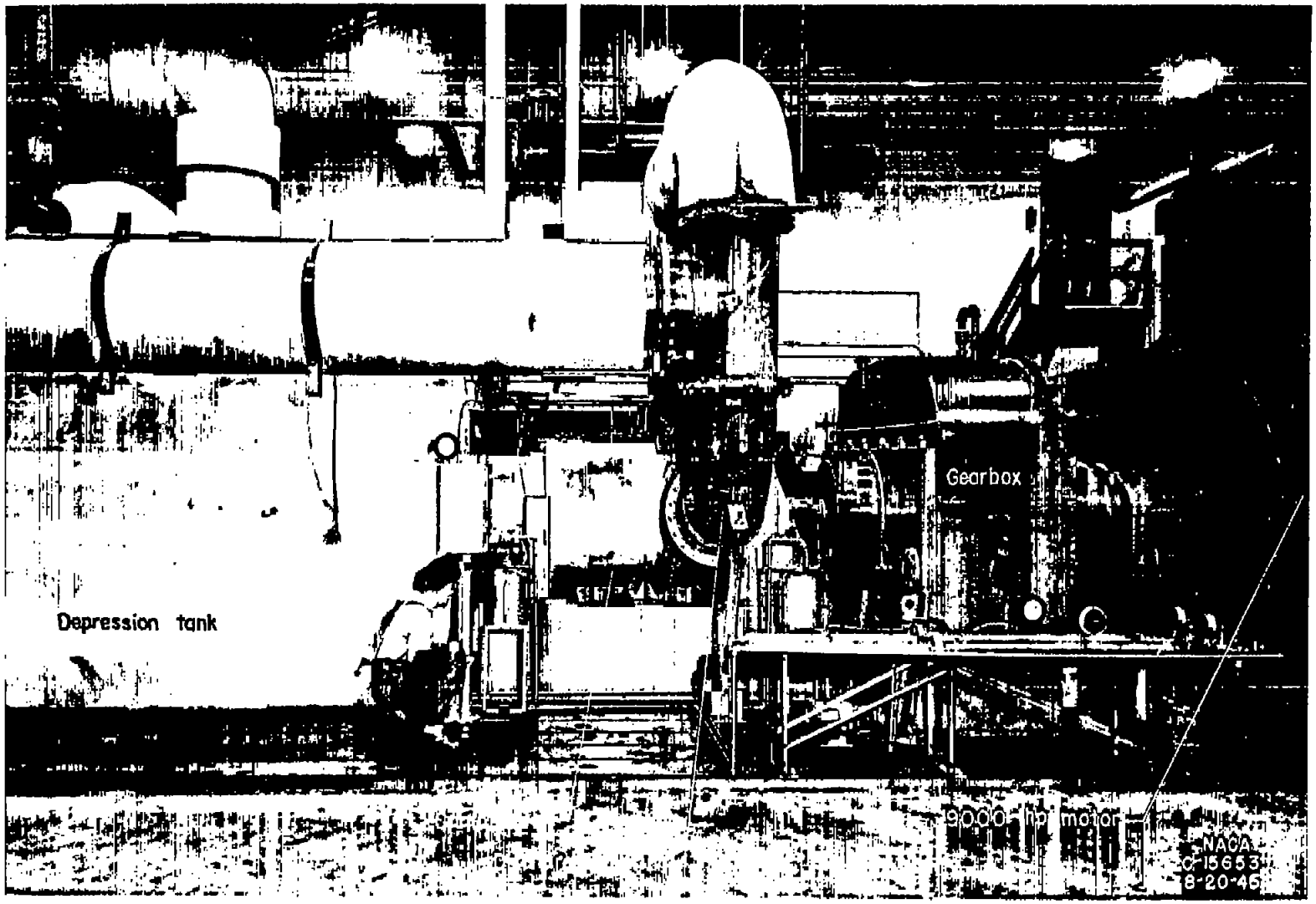

Figure 4. - Setup for investigating performance of X24C-2 axial-flow compressor.

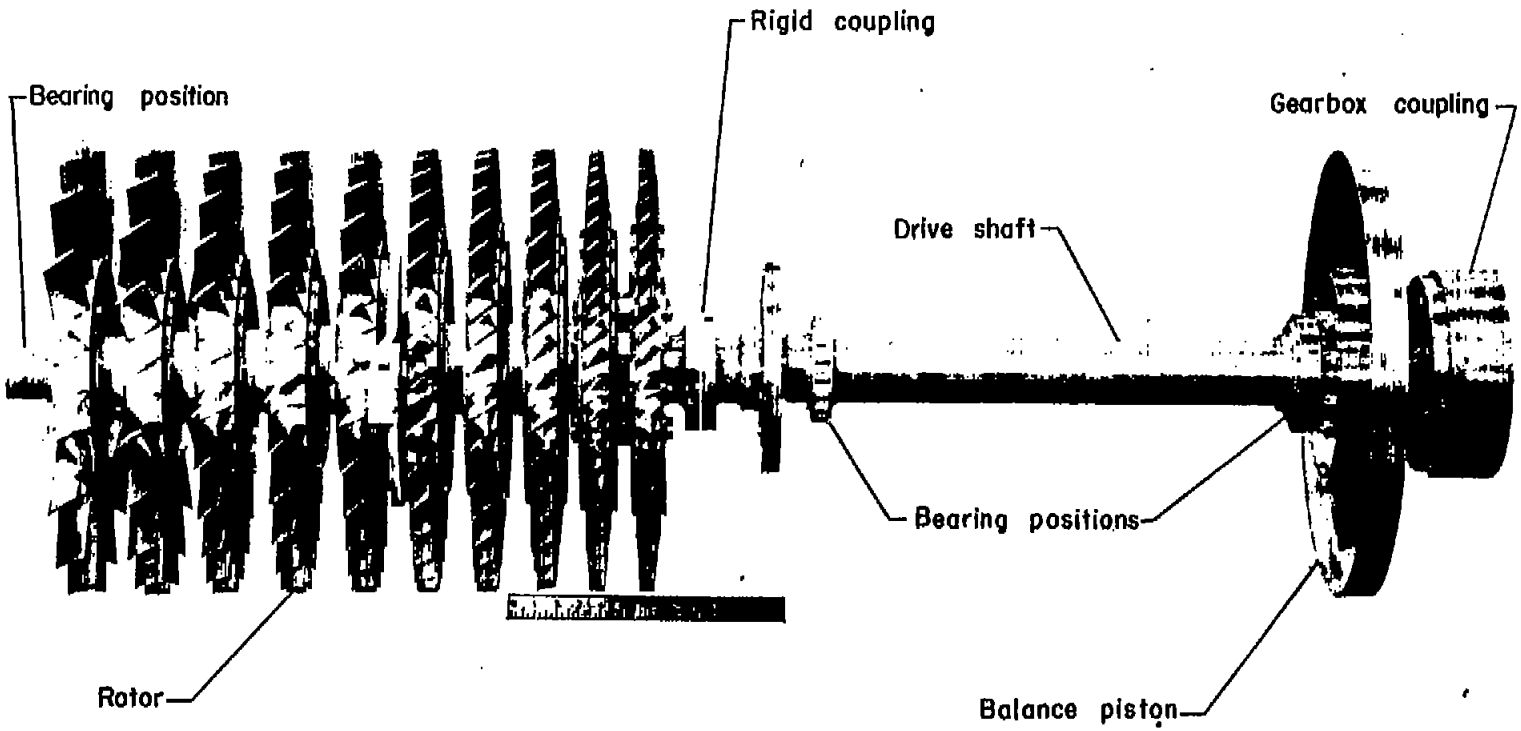

NACA
C-15992
10-10-46

Figure 5. - Compressor rotor and drive-shaft assembly.

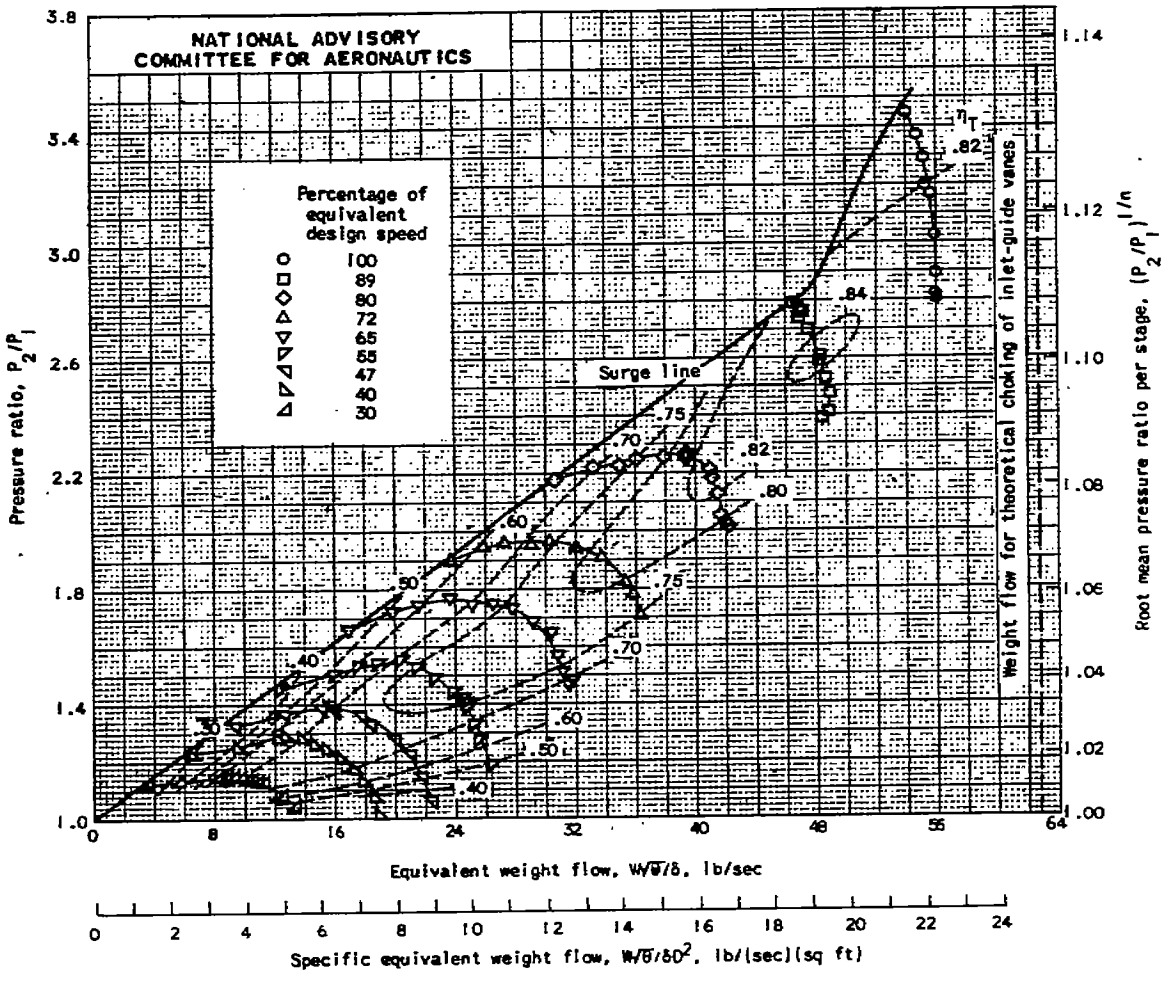

(a) All speeds investigated.

Figure 6. - Variation of over-all pressure ratio and root mean pressure ratio per stage with equivalent weight flow and specific weight flow. No diffuser; inlet total pressure for all speeds except equivalent design speed, 1485 pounds per square foot (21.0 in. Hg abs.); inlet total pressure for equivalent design speed, 1379 pounds per square foot (19.5 in. Hg abs.); inlet total temperature, 538° R.

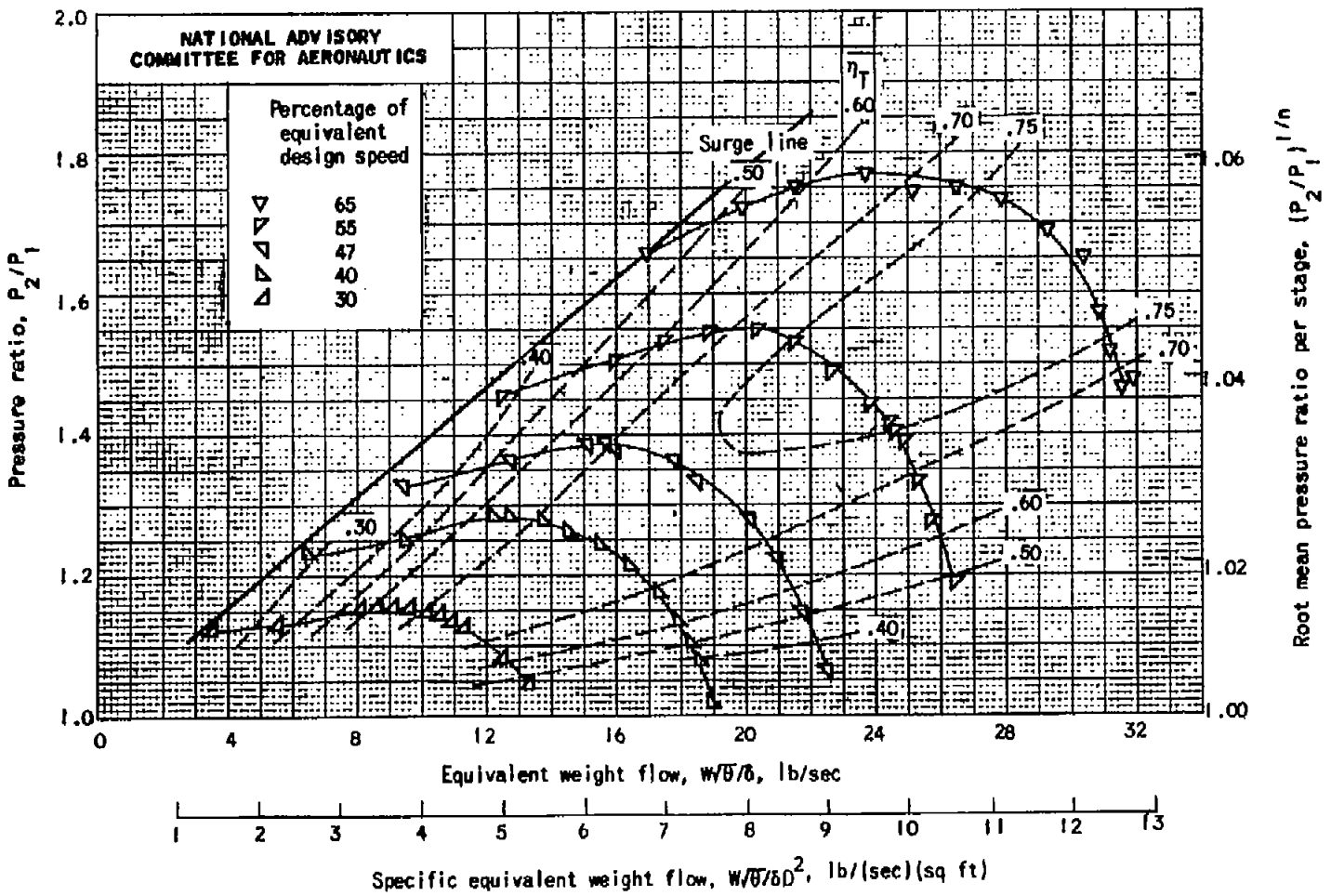

(b) Low percentages of equivalent design speed.

Figure 6. - Continued. Variation of over-all pressure ratio and root mean pressure ratio per stage with equivalent weight flow and specific weight flow. No diffuser; inlet total pressure for all speeds except equivalent design speed, 1485 pounds per square foot (21.0 in. Hg abs.); inlet total pressure for equivalent design speed, 1379 pounds per square foot (19.5 in. Hg abs.); inlet total temperature, 538° R.

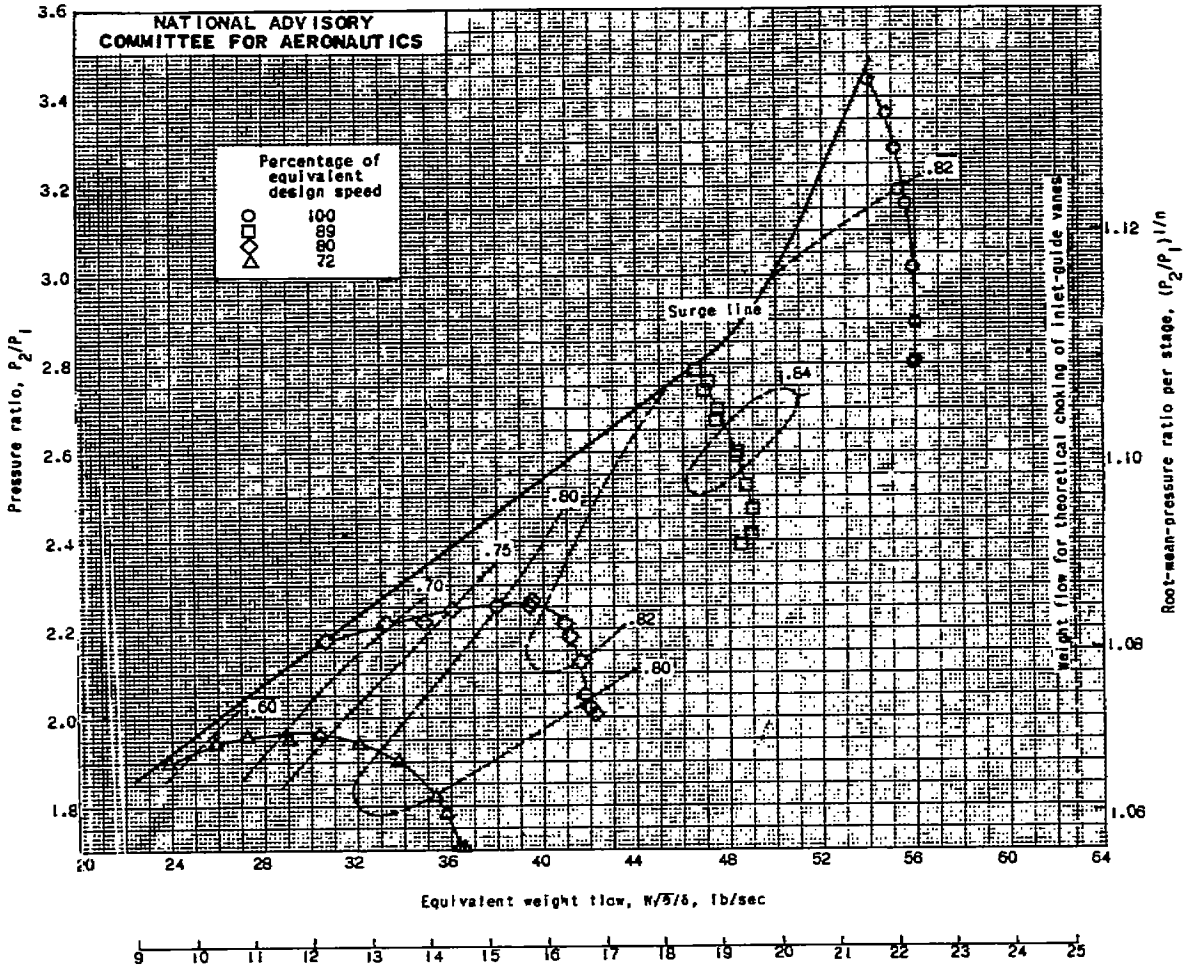

(c) High percentages of equivalent design speed.

Figure 6. - Concluded. Variation of over-all pressure ratio and root-mean-pressure ratio per stage with equivalent weight flow and specific weight flow. No diffuser; inlet total pressure for all speeds except equivalent design speed, 1485 pounds per square foot (21.0 in. Hg abs.); inlet total pressure for equivalent design speed, 1379 pounds per square foot (19.5 in. Hg abs.); inlet total temperature, 538° R.

[redacted]

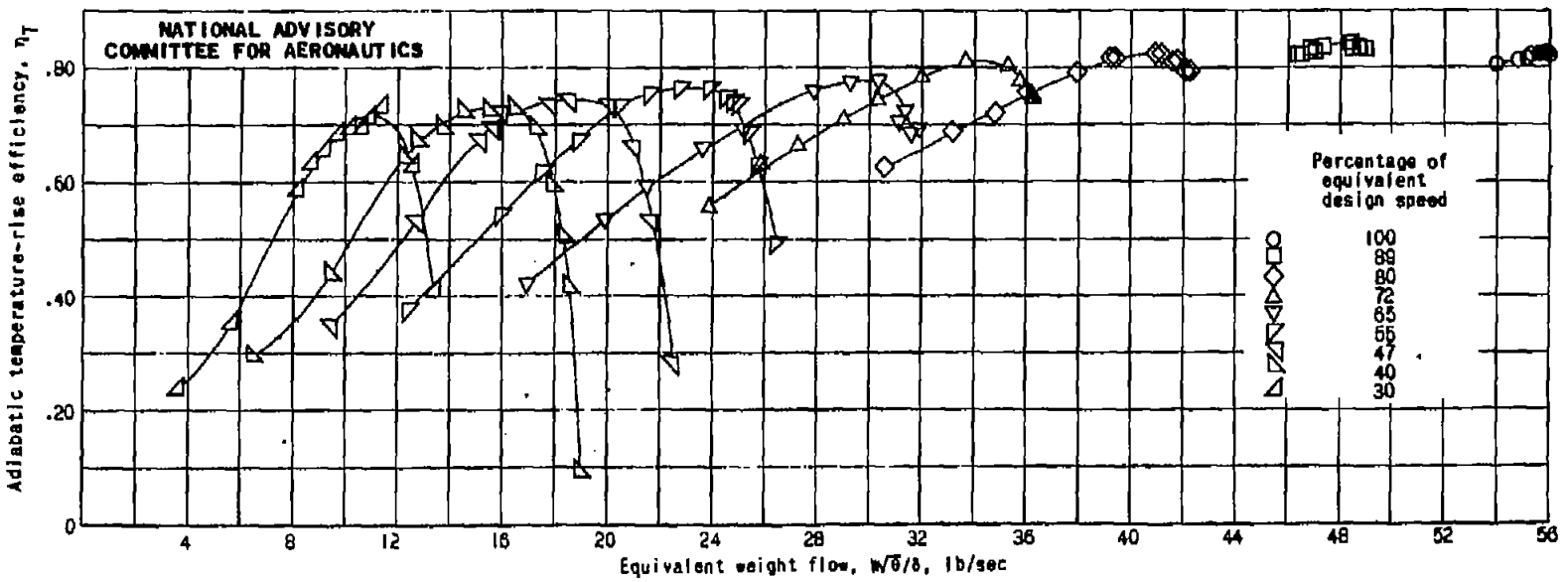

Figure 7.- Variation of adiabatic temperature-rise efficiency with equivalent weight flow. No diffuser; inlet total pressure for all speeds except equivalent design speed, 1485 pounds per square foot (21.0 in. Hg abs.); inlet total pressure for equivalent design speed, 1379 pounds per square foot (19.5 in. Hg abs.); inlet total temperature, 538° R.

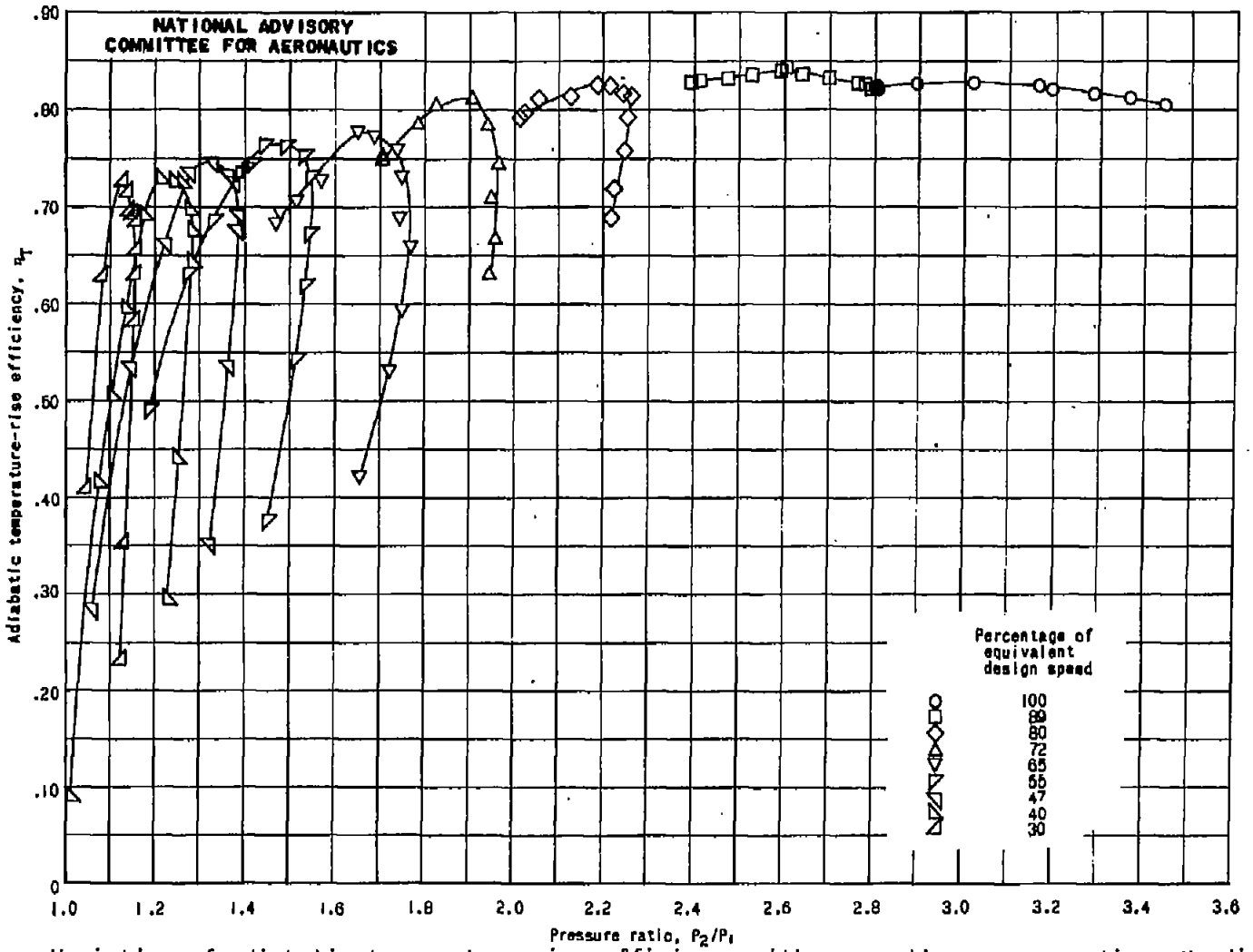

Figure 8. - Variation of adiabatic temperature-rise efficiency with over-all pressure ratio. No diffuser; inlet total pressure for all speeds except equivalent design speed, 1485 pounds per square foot (21.0 in. Hg abs.); inlet total pressure for equivalent design speed, 1379 pounds per square foot (19.5 in. Hg abs.); inlet total temperature, 538° R.

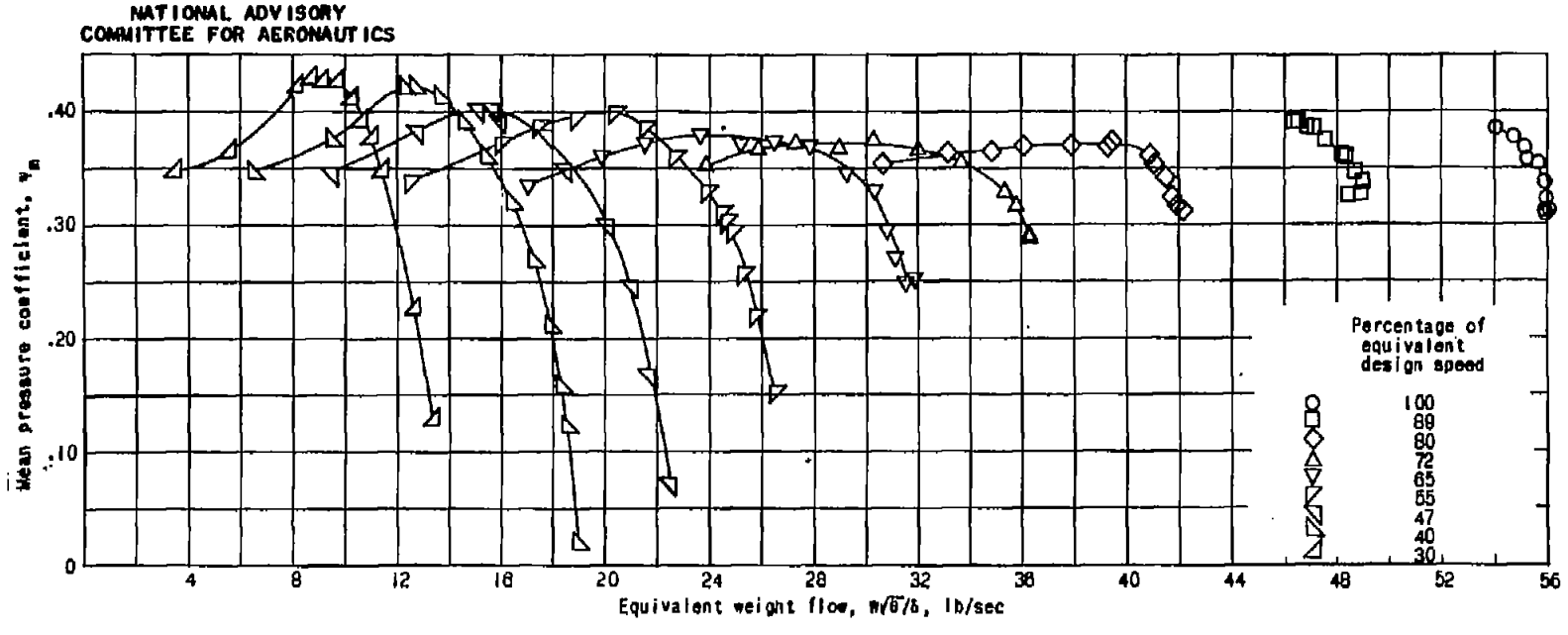

Figure 9. - Variation of mean pressure coefficient with equivalent weight flow. No diffuser; inlet total pressure for all speeds except equivalent design speed, 1485 pounds per square foot (21.0 in. Hg abs.); inlet total pressure for equivalent design speed, 1379 pounds per square foot (19.5 in. Hg abs.); inlet total temperature, 538° R.

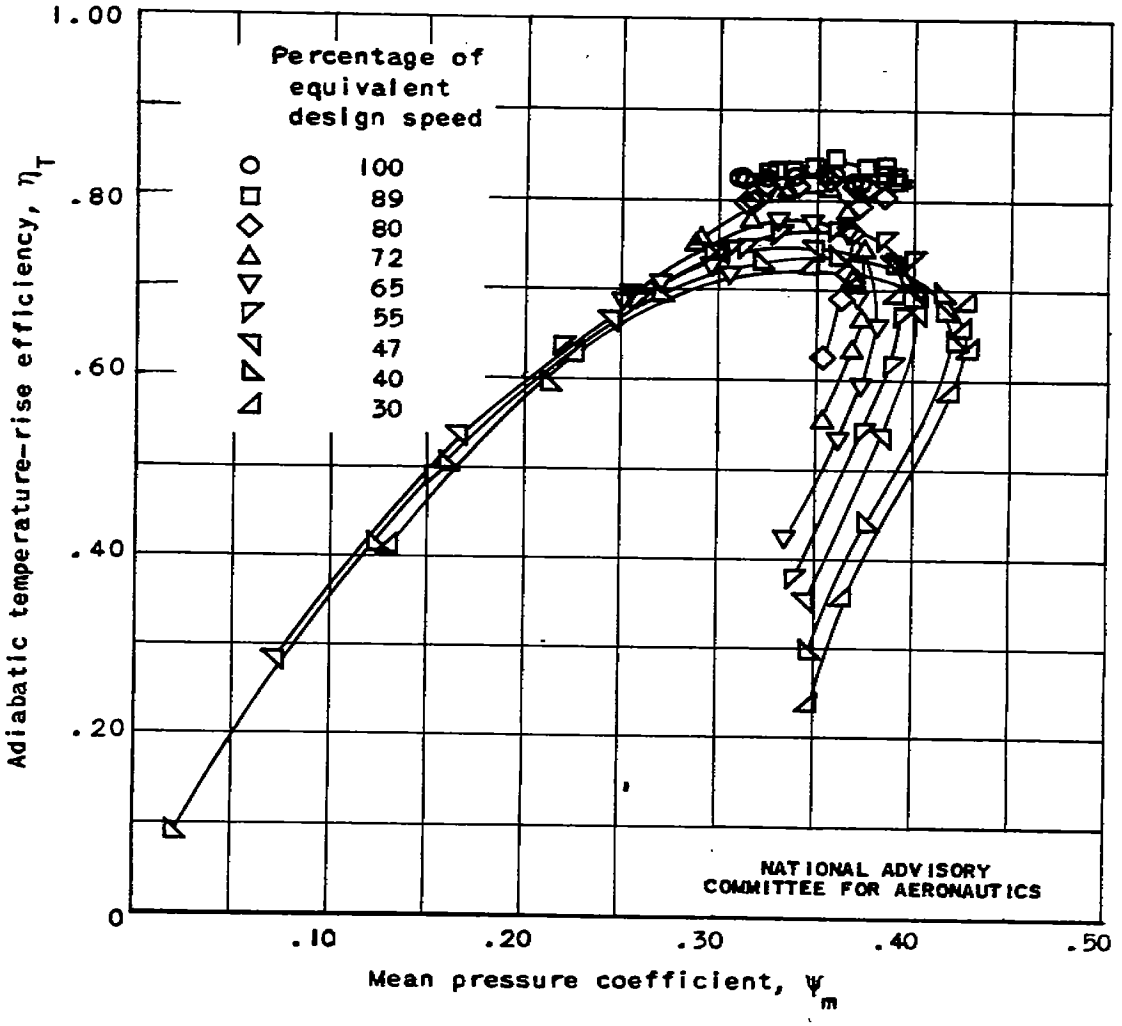

Figure 10. – Variation of adiabatic temperature-rise efficiency with mean pressure coefficient. No diffuser; inlet total pressure for all speeds except equivalent design speed, 1485 pounds per square foot (21.0 in. Hg abs.); inlet total pressure for equivalent design speed, 1379 pounds per square foot (19.5 in. Hg abs.); inlet total temperature, 538° R. (Cross plot of figs. 7 and 9.)

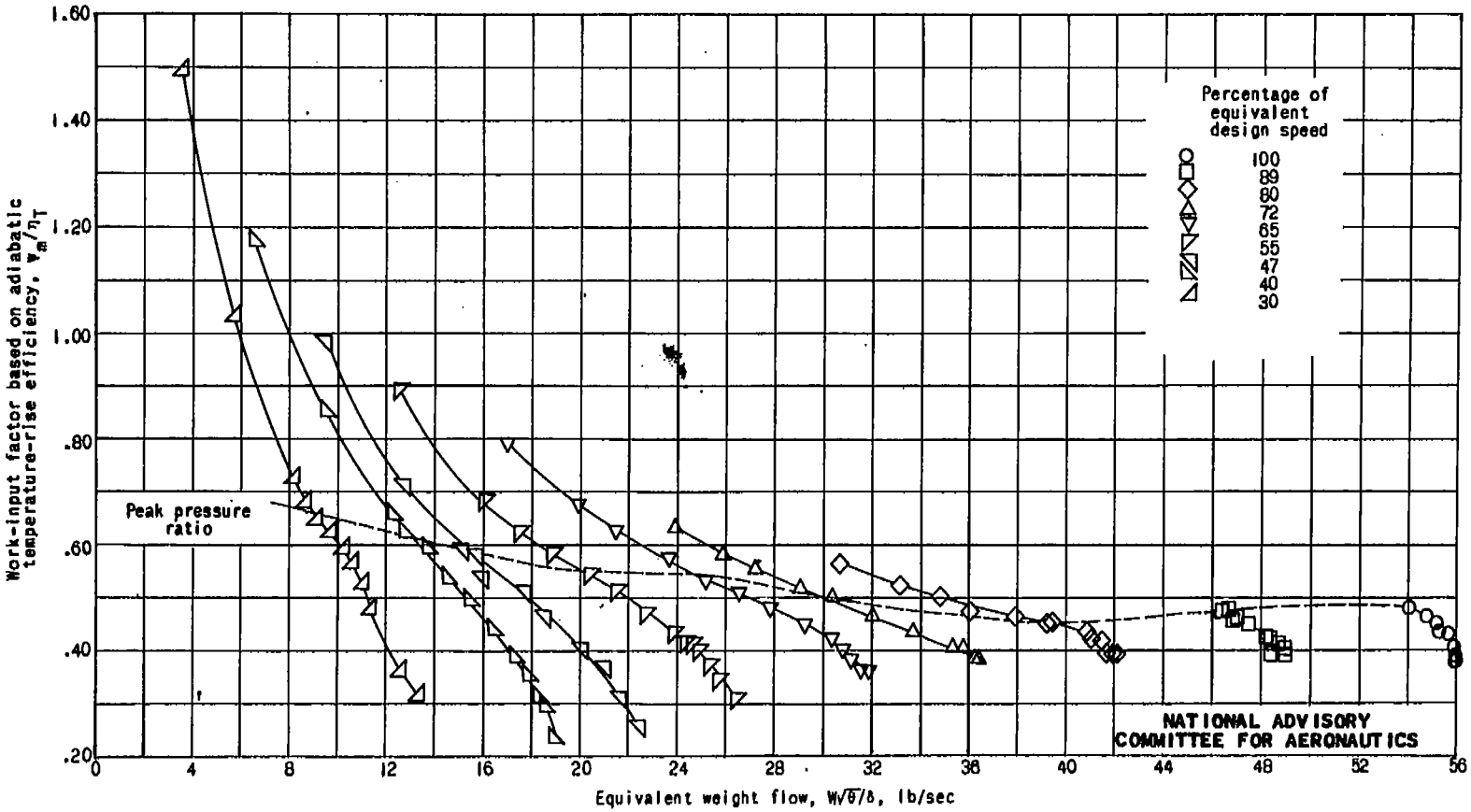

Figure 11. - Variation of work-input factor based on adiabatic temperature-rise efficiency with equivalent weight flow. No diffuser; inlet total pressure for all speeds except equivalent design speed, 1485 pounds per square foot (21.0 in. Hg abs.); inlet total pressure for equivalent design speed, 1379 pounds per square foot (19.5 in. Hg abs.); inlet total temperature, 538° R.

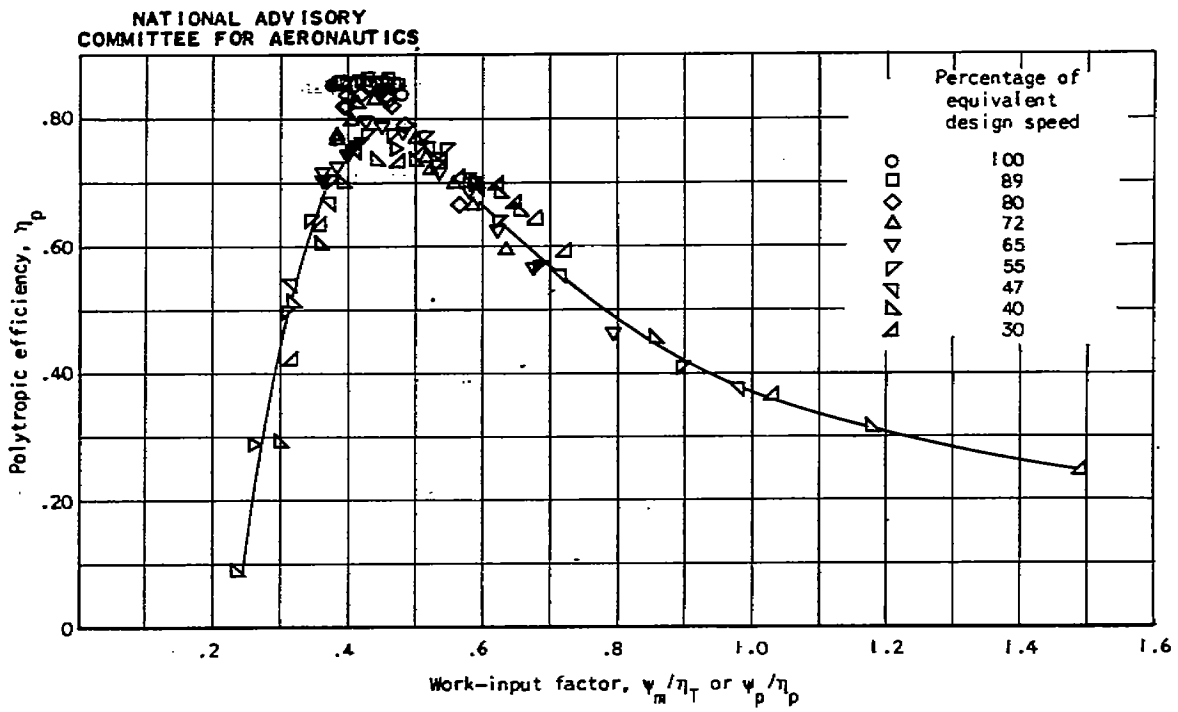

Figure 12. - Variation of polytropic efficiency with work-input factor. No diffuser; inlet total pressure for all speeds except equivalent design speed, 1485 pounds per square foot (21.0 in. Hg abs.); inlet total pressure for equivalent design speed, 1379 pounds per square foot (19.5 in. Hg abs.); inlet total temperature, 538° R.

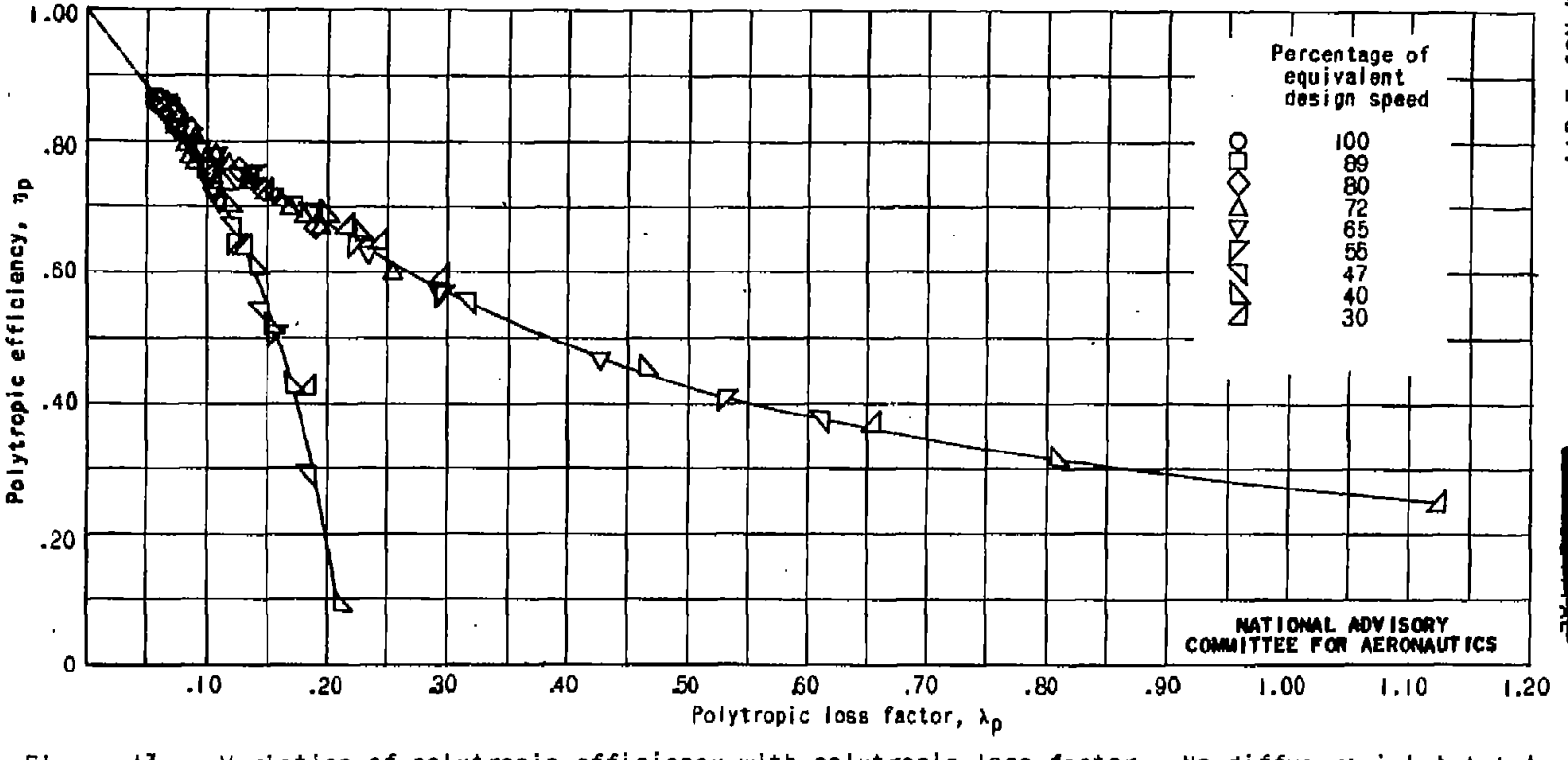

Figure 13. - Variation of polytropic efficiency with polytropic loss factor. No diffuser; inlet total pressure for all speeds except equivalent design speed, 1485 pounds per square foot (21.0 in. Hg abs.); inlet total pressure for equivalent design speed, 1379 pounds per square foot (19.5 in. Hg abs.); inlet total temperature, 538° R.

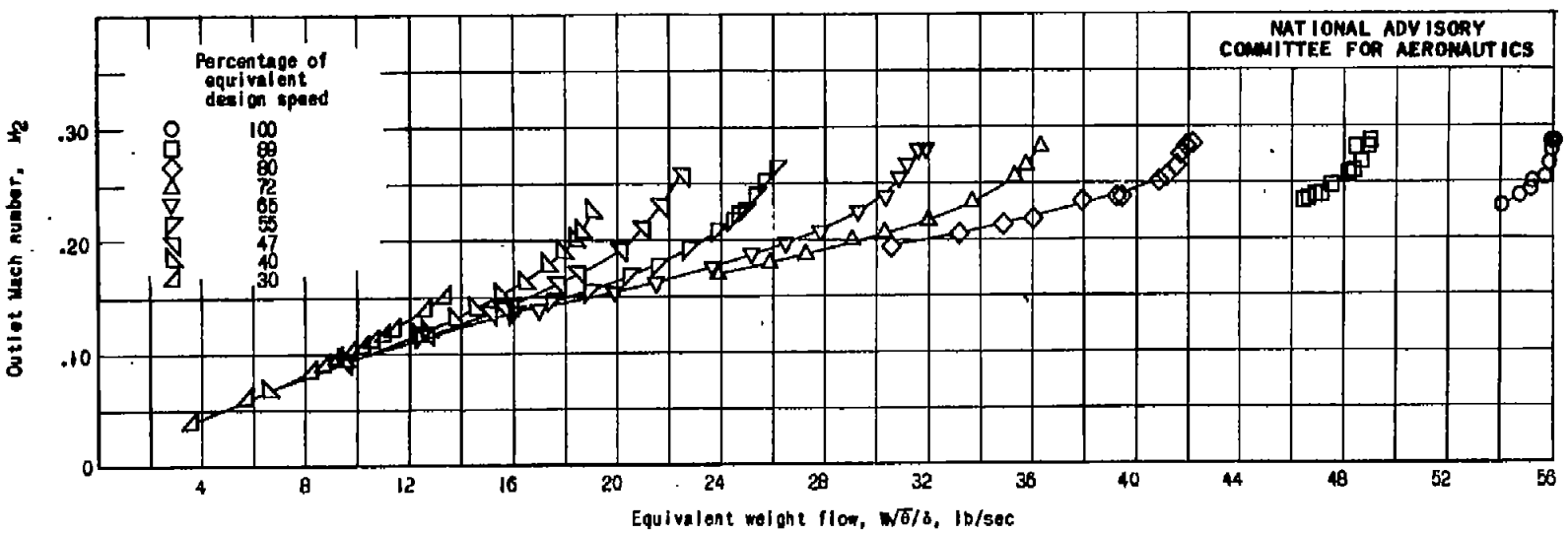

Figure 14. - Variation of outlet Mach number with equivalent weight flow. No diffuser; inlet total pressure for all speeds except equivalent design speed, 1485 pounds per square foot (21.0 in. Hg abs.); inlet total pressure for equivalent design speed, 1379 pounds per square foot (19.5 in. Hg abs.); inlet total temperature, 538° R.

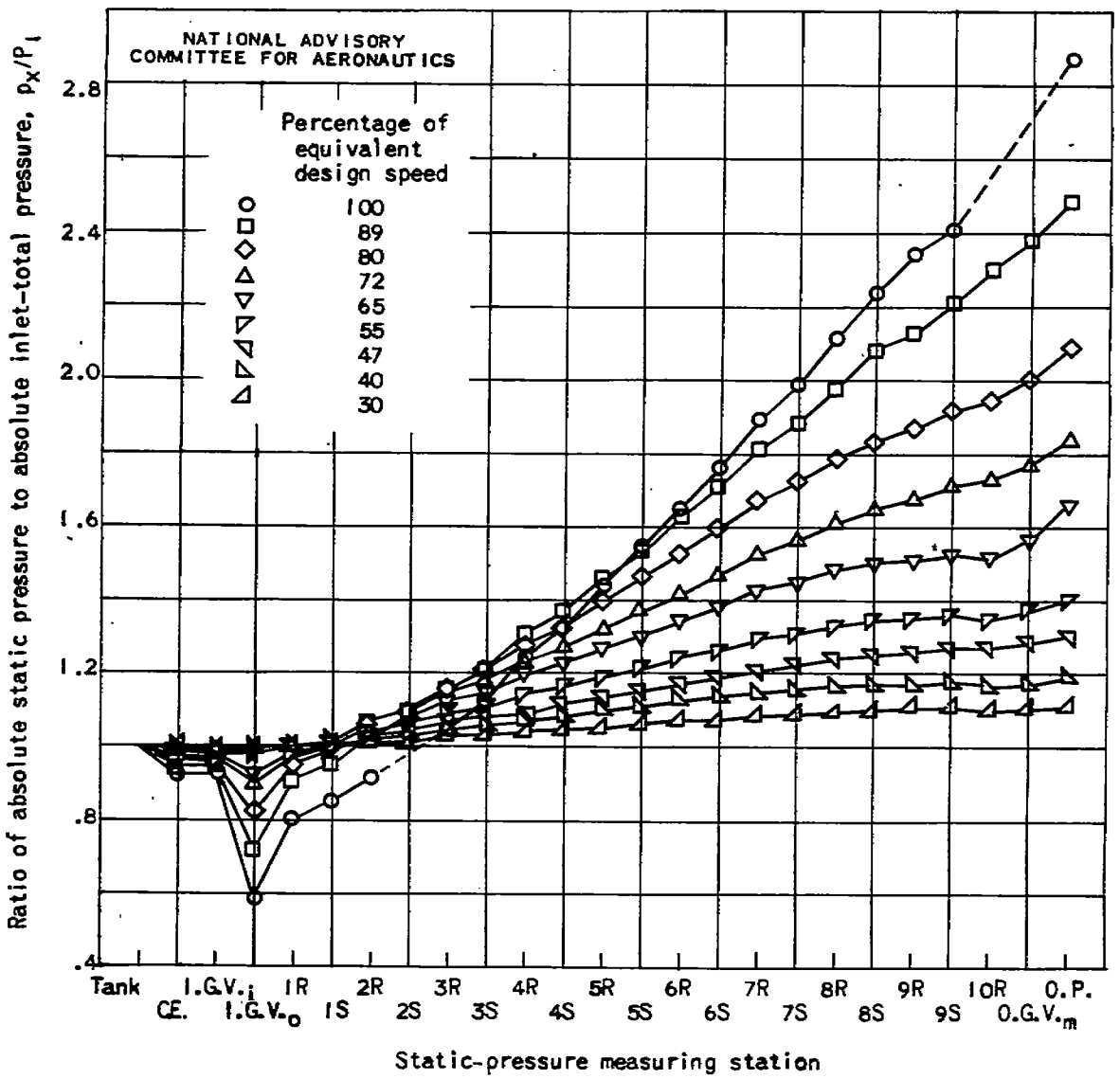

Figure 15. - Variation of static pressure along compressor casing for peak efficiency conditions. No diffuser; inlet total pressure for all speeds except equivalent design speed, 1485 pounds per square foot (21.0 in. Hg abs.); inlet total pressure for equivalent design speed, 1379 pounds per square foot (19.5 in. Hg abs.); inlet total temperature, 538° R; compressor entrance, C.E.; inlet-guide vanes, I.G.V.; rotor blades, R; stator blades, S; between two rows of outlet-guide vanes, O.G.V.$_m$; outlet passage, O.P; inlet, i; outlet, o.

[redacted]

NASA Technical Library
3 1176 01425 9619

Authors (2)
Compressors, Axial-flow
[illegible], Jet-Turbo